CrystEngComm

Accepted Manuscript

ROYAL SOCIETY OF CHEMISTRY

www.rsc.org/crystengcomm

Cite this: DOI: 10.1039/c0xx00000x

www.rsc.org/xxxxxx

ARTICLE TYPE

Solvothermal Synthesis of Co_3O_4/Al_2O_3 Hollow Core-shell Microspheres for Catalytic Oxidation of CO

Liangmiao Zhang, *[a] Taiang Liu,[b] Xin Zhao,[b] Na Qian,[b] Pan Xiong,[b] Wenjing Ma,[b] Wencong Lu,*[b]

Yanfeng gao[c] and Hongjie Luo[a,c]

A facile template-free solvothermal strategy has been developed to synthesize uniform and hollow core-shell Co_3O_4/Al_2O_3 microspheres composed of numerous tiny nanorods. The morphology, structure, and composition of the spheres are investigated using field-emission scanning electron microscopy (FESEM), transmission electron microscopy (TEM), Fourier transform infrared spectra (FTIR), Raman spectra, H_2-temperature programmed reduction (H_2-TPR) and X-ray diffraction analysis (XRD). The specific surface area and pore-size distribution of the obtained products as determined by gas-sorption measurements show that the core-shell microspheres exhibit high surface area and porosity properties. The formation of hollow structure involves a trisodium citrate (TSC)-assisted Ostwald ripening process. The structure and influences factors that govern the shape evolution of core-shell Co_3O_4/Al_2O_3 microspheres have been carefully studied, such as Co wt% amount, TSC/Al ratio and temperature. Catalytic activities of the as-prepared core-shell Co_3O_4/Al_2O_3 microspheres are evaluated by the CO catalytic oxidation. The high performance may be attributed to its large specific surface area, high porosity, mesoporous structure.

1. Introduction

Hollow and core-shell nanocrystals with controlled hollow interior and shell thickness represent a class of important nanostructured materials, because of their large surface area and low material density, which can serve as ideal building blocks for fabrication of lightweight structural materials and in promising applications for nanoreactors, drug delivery, and catalysis.[1-2] The most popular approach for the synthesis of hollow nanoparticles is the template methods.[3-4] The templates include hard-core templates [5-9] (such as PS spheres, PSA latex, resin spheres, silica, carbon, and the colloid metal oxide particles) and soft-core templates [10-12] (such as vesicles, emulsions, droplets, micelles, and large molecule aggregates). However, in some cases, the conventional template-based strategy seem to be inconvenient because complete template removal is needed, which means a much more complicated process including the selection of appropriate solvent or calcination at elevated temperature, especially when the templates themselves are difficult to fabricate in large quantity. Recently, appropriate chemical transformations, such as via the interior corrosion[13-14], nanoscale Kirkendall effect [15-16], Ostwald ripening [17-18] and surface-protected etching, have been developed to synthesize various hollow and core-shell micro/nanospheres. Recently, some efforts have been devoted to the synthesis of inorganic hollow structures with spherical and nonspherical morphologies.[19] For example, core-shell and hollow zeolite analcime icositetrahedra has been successfully synthesized by a reversed crystal growth process via oriented aggregation of nanocrystallites and recrystallization from surface to core. [20] Li [21] *et al.* has reported the fabrication of core-shell spheres with unique urchin-like morphology by solvothermal reaction, which exhibit greatly enhanced photocatalytic activity attributed to their unique sphere-in-sphere structure. Single-crystalline Cu_2O hollow nanocubes were fabricated via a precursor hydrolysis process by the assistance of PEG.[22] In my previous work [23-24], we have reported a facile "hydrothermal-assisted dissolution-renucleation" route to synthesize hierarchical hollow and sphere-in-sphere AlOOH microspheres, which are demonstrated to be attractive candidate materials for organic waste water treatment. However, the above-mentioned methods are usually just suitable for certain specific metal oxide hollow structure, and no clear evidence indicates that it can be applied to general metal oxides, especially the composite oxides. Therefore, it is still a big challenge to fabricate composite oxides hollow structures by a general and facile route.

Co_3O_4/Al_2O_3 nanocomposites have been widely used as pigments, sensors, catalysts, electrode materials for supercapacitors due to their interesting properties, such as highly thermal stability, high acidity, unique pore structure, and large surface area, etc.[25-28] Although many approaches have been explored to prepare Co_3O_4/Al_2O_3 nanocomposites, most of the reported methods, eg., sol-gel process, co-precipitation, incipient-wetness impregnation, and hydrothermal or solvothermal method, are focused on the fabrication of Co_3O_4/Al_2O_3 nanocrystallines. [29-36] Less effort has been focused on the novel 3D structures with large BET surface area and outstanding catalytic properties.

Herein, we demonstrate a facile and efficient strategy for the synthesis of hollow core-shell Co_3O_4/Al_2O_3 microarchitecture, and its catalytic performance was tested for the catalytic oxidation of CO. To the best of our knowledge, this is the first report on synthesis of

Co_3O_4/Al_2O_3 hollow core-shell microspheres with large BET surface area and outstanding catalytic properties. Furthermore, the effects of reaction parameters on the formation of nanostructures and their formation mechanism were also discussed.

2. Experimental Section

2.1 Materials Synthesis. All chemical reagents were analytical grade and purchased from Shanghai Chemical Reagent Company (P. R. China) without further purification. In a typical procedure for the preparation of Co_3O_4/Al_2O_3 with 15wt% Co, 2 mmol of $Al(NO_3)_3 \cdot 9H_2O$ was dissolved in 20 mL of distilled water. Then 20 mL of acetone was added slowly to this solution. To this mixture was added 0.5 mmol of the TSC (trisodium citrate dehydrate, $C_6H_5Na_3O_7 \cdot 2H_2O$), and the resulting solution was further stirred vigorously for 30 min. And then an appropriate amount of $CO(NH_2)_2$ (0.0183g) and 0.9ml $Co(NO_3)_2$ (0.02g/ml) were added into the above solution. Subsequently, the mixed solution was transferred into a 50 mL Teflon-lined stainless steel autoclave, sealed, and maintained at 200 ^oC for 24h. After being cooled to the room temperature, the products were isolated by centrifugation and washed with deionized water and absolute ethanol several times, followed by drying at 60 ^oC overnight. All samples were calcined at 350 ^oC for 1h and subsequently at 500 ^oC for 3h under static air in a muffle furnace. Four sets of compositions with nominal Co wt% of 5%, 10%, 15%, 25% were prepared following the similar procedure (labeled as S-5, S-10, S-15, S-25 for simplicity).

2.2 Characterization of the samples. The XRD patterns were recorded on a Japan Rigaku D/Max-RB X-ray diffractometer with Cu Kα radiation (λ=1.54178 Å). A small amount of products were ultrasonically dispersed in alcohol and deposited on copper grids coated with ultra-thin films for transmission electron microscopy (TEM, JEM-2010F, JEOL) measurements. Field emission scanning electron microscopy (FESEM, JSM-6700F, JEOL, Japan) was employed to analyze the morphology, and the chemical components of the products were measured with an energy dispersive X-ray spectrometer (EDS). Fourier transform infrared (FTIR) spectra were obtained on an AVATAR370 spectrometer. Raman spectra of the samples were collected with an invia micro-Raman system with 632.8 nm diode laser excitation on a 300 lines/mm grating at room temperature. The cobalt content in all the samples was determined by inductively coupled plasma atomic emission spectroscopy (ICP−AES) on an ICPS-7510 instrument. BET surface areas of the samples were measured by N_2 adsorption-desorption at -196 ^oC on a micromeritics ASAP 2020 instrument, and were calculated by the Brunauer-Emmett-Teller (BET) method. H_2-temperature programmed reduction (H_2-TPR) was performed in a quartz U-tube with 50 mg catalyst (40-60 mesh). After the sample was pretreated in N_2 at 500 ^oC for 30 min, it was cooled down to room temperature, and then the mixture of 10 vol% H_2/N_2 (25 cm^3 min^{-1}) was used instead of N_2. The heating rate was 10 ^oC min^{-1}. The uptake amounts of H_2 were measured by a thermal conductivity detector (TCD).

2.3 Catalytic activity testing. The activity of catalyst for CO oxidation was evaluated in a fixed-bed reactor at atmosphere pressure, and 300 mg catalyst (40-60 mesh) was used. A gas mixture (3% CO, 12% O_2, and 85% N_2) was then introduced into the reactor at a flow rate of 40 cm^3 min^{-1}. The composition of the gas exiting the reactor was monitored by gas chromatography, to determine both the removal of CO and the formation of CO_2. All the catalytic results were repeated three times at a given temperature. An online gas chromatograph (GC1609) equipped with a thermal conductivity detector (TCD) was used to analyze the outlet stream after the catalyst bed temperature stabilized at the settled value for 15 min to obtain the steady state. The conversion of CO to CO_2 over the samples was measured at various temperatures. T_{50} and T_{90} are defined as the temperatures at which the conversion of CO to CO_2 reached 50% and 90%, respectively.

3 Results and Discussion

3.1 Phase, Morphology and Texture Properties. Parts A, B, C, and D of Figure 1 display typical TEM images of the hollow core-shell microparticles of crystalline Co_3O_4/Al_2O_3 microspheres obtained with different Co amounts, illustrating a hollow and core-shell morphology with single particle size of 2-4 μm. The hollow structure is evident from the obvious contrast between their edges and centers and broken particles (Fig. 2a). The interesting nanostructure of hollow core-shell microspheres was further corroborated by scanning electron microscopy (SEM). The thickness of the shells is 100-200 nm. It should be mentioned that a low amount of cobalt ions did not change the phase, morphology, or crystallization of the resulting samples because of their very similar ionic radii. We can see that it is obvious similarity in the size and shape. The high-magnification TEM image, f of Figure 1, shows that the as-synthesized shells of the microspheres are random assembled by numerous nanorods (50-100 nm in length and 5-10 nm in diameter) intercrossed with each other. This indicates that most of the pores within the samples might be mesoporous. The content of Co is analysized by ICP-AES technique, which is also shown in Table 1. According to the analysis results of EDS (Fig.2b and c), the average Co contents of the shell and the core of the sample S-10 are 6.78wt% and 6.63wt%, respectively. This is basically in accord with the result of element analysis of ICP-AES.

Table 1 BET Surface Area, Pore Volumes and Crystallite Sizes of the Co_3O_4/Al_2O_3 samples.

samples	The content of Co determined by ICP	Co_3O_4 size [a] (nm)	BET surface area (m^2g^{-1})	Pore volume (cm^3g^{-1})	Average pore diameter (nm)
S-5	4.8%	n.d.[b]	274.1	0.55	6.9
S-10	7.0%	13.8	264.7	0.50	6.2
S-15	12.3%	16.0	254.0	0.50	6.5
S-25	22.5%	27.9	206.2	0.69	10.7
Ref.43(8wt% Co)	n.g.[c]	n.g.[c]	203.0	0.37	3.1

[a] Calculated through the XRD patterns by Scherrer equation. [b] n.d.: not determined. [c] n.g.: not given.

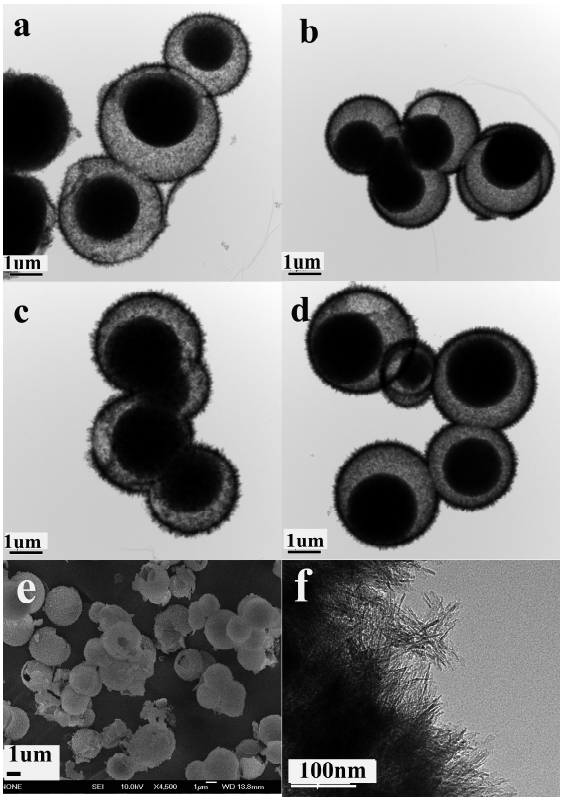

Fig. 1 Low-magnification TEM (a-d) and SEM (e) images of hollow core-shell Co_3O_4/Al_2O_3 microspheres. (a) S-5; (b) S-10, (c) S-15; (d) S-25. (f) the high-magnification of the shell for S-15.

XRD patterns of the hollow core-shell Co_3O_4/Al_2O_3 microspheres by solvothermal method are shown in Figure 3. As can be seen, the pattern of sample S-25 has relatively high diffraction intensities of phase such as Co_3O_4 and/or $CoAl_2O_4$ and γ-Al_2O_3 phase. [37] The S-10 and S-15 samples have the same diffraction pattern as the S-25 samples, but with much lower intensities, and no γ-Al_2O_3 phase can be detected. The XRD peak breadth for the S-5 sample is even broader, which reveals a nanosized crystalline state in this sample. This reducing phenomenon is also found with reducing the calcination temperatures (See Figure S1). After increasing the amount of cobalt, a new sharp reflex at 38.68 is observed in the XRD pattern of S-25, which may corresponds to $CoAl_2O_4$ crystallites. [38] Besides the reflexes characteristic of γ-Al_2O_3 and the reflex at 38.68, new reflexes at 2θ = 31.58, 45.58 and 65.78 corresponding to Co_3O_4 (JCPDF: 43-1003) crystallites are observed. This result implies that Co_3O_4 is formed in S-25. No characteristic peaks of the CoO phase at 2θ = 34.1°, 39.5°, 57.2°, and 68.4° are observed.

The crystallite sizes of Co_3O_4 in all samples are calculated from the Co_3O_4 (311) diffraction peak by the Scherrer equation and shown in Table 1. It can be seen that the crystallite size of S-10 is 13.8 nm, and only half crystallite sizes (27.9 nm) of S-25 sample. For the S-5 sample, because of a relatively small crystalline between the metal Co and the AlOOH in the process of solvothermal process, resulting in no obvious diffraction peaks appeared. It is difficult to establish the chemical and structural phases for the four samples based on XRD characteristics alone because Co_3O_4 and $CoAl_2O_4$ both have cubic spinel structure with almost identical diffraction peak positions. [39-41] Nonetheless, the difficulty in resolving these two phases can be overcome by FTIR and Raman techniques.

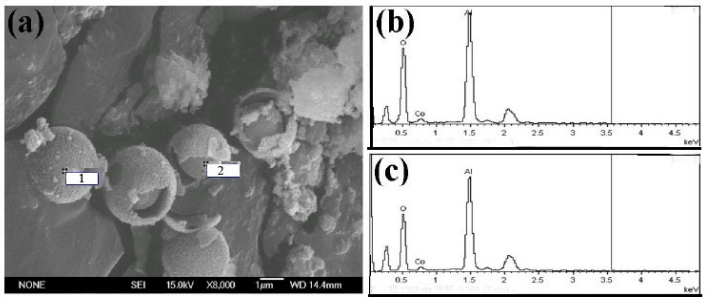

Fig. 2 SEM image (a), EDS spectrum of the shell (b) and the core (c) in the S-10 sample.

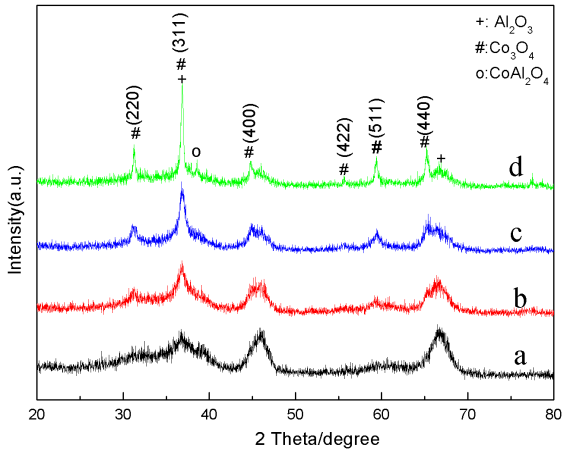

Fig. 3 XRD patterns of the samples (a) S-5, (b) S-10, (c) S-15, (d) S-25. (#)Co_3O_4; (O) $CoAl_2O_4$ and (+) γ-Al_2O_3.

Figure S2 shows the FTIR spectrum of the four core-shell samples with different Co-loadings. The wide band in 3600-3300 cm^{-1} and the weak bond at 1640 cm^{-1} were attributed to hydroxyl stretching and bending mode of absorbed water, respectively. Two absorption bands at 582 and 670cm^{-1} are observed in the IR spectrum of cobalt oxide, which is in accordance with the stretching vibration of metal-oxide bond in the Co_3O_4 spinel lattice. As shown in Figure S2, the intensity of the two stretching vibration band is changed in the order of S-5<S-10<S-15<S-25, which indicates that the strength of the Co-O bond with much Co amount is stronger and more difficult to be reduced than those with less cobalt catalysts. The results above are consistent with the TPR results (Figure 10); that is, the Co^{3+} reduction temperatures shift to higher temperature in the same order as their IR spectra intensify effect for the four Co_3O_4/Al_2O_3 core-shell samples.

Figure S3 shows the Raman spectra of samples obtained. Five obvious Raman peaks are located at 188, 476, 516, 615, and 683 cm^{-1}.They correspond to 3 F_{2g}, 1 E_g and 1 A_{1g} Raman active modes of the Co_3O_4 nanocrystals, while the characteristic peaks of Al_2O_3 could not be detected. All of the Raman peaks on Co_3O_4/Al_2O_3 broadened, which associated with the lattice distortion or residual stress of the spinel structure [33]. The results are accorded with the XRD results, which show that part of Co_3O_4 entered the lattice of Al_2O_3 over Co_3O_4/Al_2O_3 samples, the interaction between Co_3O_4 and Al_2O_3 aroused the lattice distortion and lattice defect.

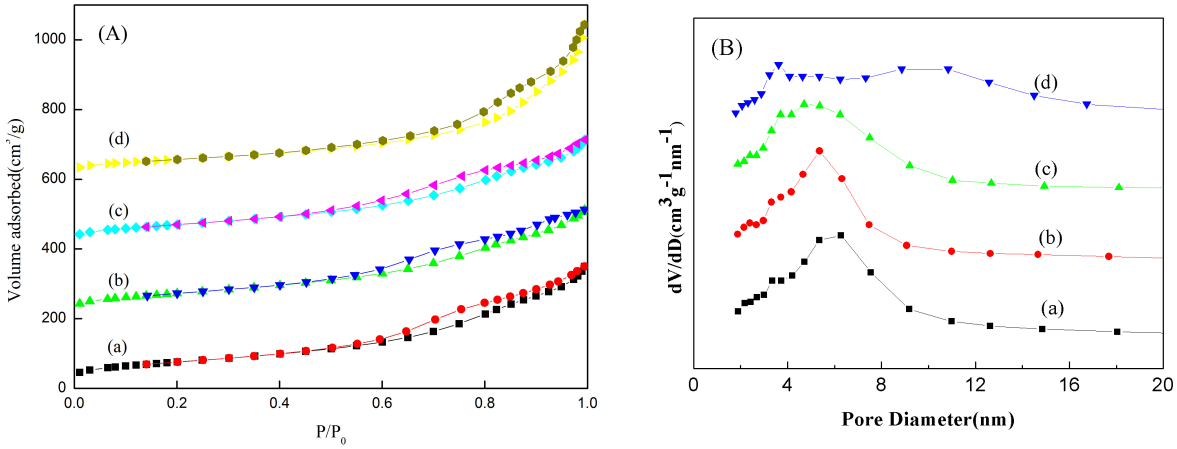

Fig. 4 N_2 adsorption/desorption isotherm of the samples(A) and their corresponding pore-size distribution curves (B). (a) S-5, (b) S-10, (c) S-15, (d) S-25.

In order to ascertain formation of the mesoporous structure, N_2 adsorption/desorption experiment of the samples prepared with various Co loadings was carried out. The adsorption and pore properties of the samples, as calculated from the adsorption−desorption isotherms, are listed in Table 1. The pore size distribution curves in Figure 4B also presents the same results, which were estimated by software using Barrett−Joyner−Halenda (BJH) analyses from the desorption curve of the isotherms. It can be seen from Figure 4A that all the samples exhibit typical IV-type isotherms with H1 hysteresis loops, which show the characteristics of typical mesoporous materials. [42] The specific surface areas and total pore volumes are calculated at the range of 206-274 m^2/g and 0.5-0.69 cm^3/g. The higher specific surface area of the Co_3O_4/Al_2O_3 material can be attributed to the hollow structures and will be useful to enhance the catalytic performance of the samples. As shown in Figure 4B, we can see that the pore diameters are about 6.2-10.7 nm, indicating that the shell of hollow spheres were of a porous structure, which also can be observed from the enlarged TEM image showing in Figure 1f. And the average pore size shows an obvious increase with increasing Co loadings, this change can be ascribed to the growth of crystal in the shell as confirmed by XRD. The growth of domains eliminated some porous structures, resulting in the decrease of specific surface area. The

relatively larger pore sizes (4-8 nm) were observed for all samples, which is likely beneficial to the introduction of cobalt species into the pore channel of alumina support and further distribution. Moreover, the surface area and pore structure of the core-shell Co_3O_4/Al_2O_3 microspheres is still superior to that of Co_3O_4/Al_2O_3 nanopowders prepared by Zhang [43] as shown in Table 1.

Growth Mechanism of the Hollow Core-shell Spheres.

To explain the evolution of the hollow core-shell spheres, step-dependent experiments were carried out. From Figure 5, we can see that the solid spheres changed to hollow ones with an increase of the reaction time. Parts a-h of Figure 5 show the TEM images of Co_3O_4/Al_2O_3 microspheres with 15wt% Co-loading prepared for the reaction time from 3 to 48 h with Al/TSC molar ratio of 4 and the reaction temperature of 200°C. When the time is set to 30 min, we can see that the precursor consists of solid spheres with an average diameter of 1.5-3 μm (Figure 5a). When the reaction time is up to 3-6 h, some tiny nanorods appear on the surface of the spheres (Figure 5b, c). As the reaction time is increased to 12 h (Figure 5d), an obvious gap between the core and shell developed, and the bulk core in the hollow interior could be clearly observed. These facts indicate a possible etching process that occurs inside these spheres. As the reaction further proceeds to 24 and 48h, the shape of particles has no obvious change, but the core gradually reduces until two spheres fused to one sphere with dumbbell morphology, as shown in Figure 5e-h. It indicates that as time elapses, further corrosion might occur, preferentially around the core, leading to the formation of core–shell structure. The corresponding XRD patterns (shown in Fig.6) reveal that all of the samples prepared at different reaction time are mainly AlOOH and $Co(OH)_2$ phase, and no phase transition takes place during the whole reaction process, indicating that the core-shell structures are homogeneous. The crystallinities of the products increase and the sizes of the nanogranular units grow larger gradually with prolonged the reaction time, which can be confirmed by the peak height and peak width of XRD patterns.

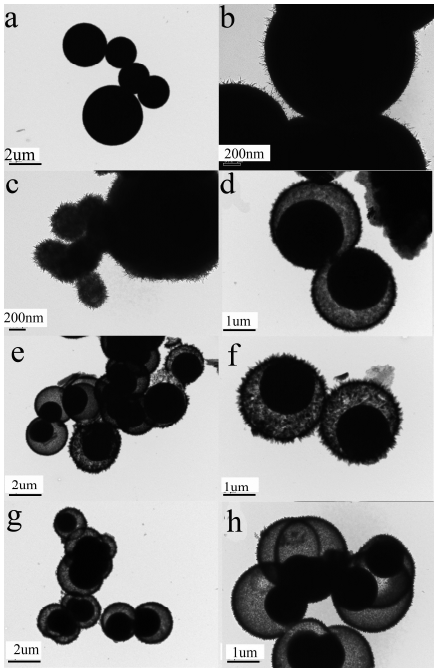

Fig. 5 TEM images of the 15wt% Co-loading sample collected at different reaction times: (a) 0.5, (b)3, (c) 6, (d) 12, (e, f) 24, and (g, h) 48 h under other reaction parameters are kept constant.

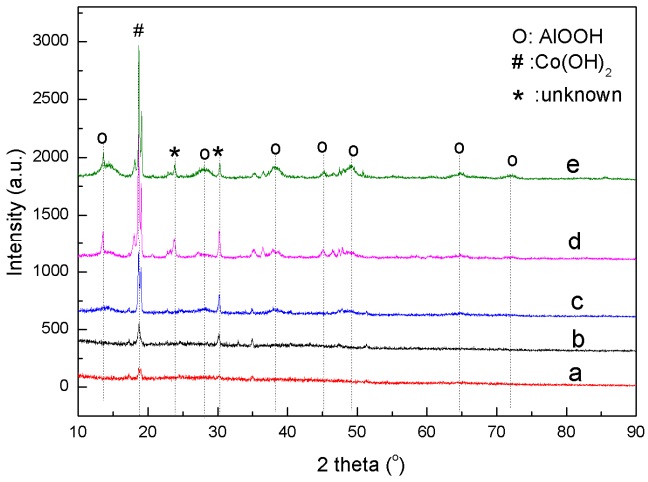

Fig.6 XRD patterns of the above samples collected at various reaction times: (a) 3h, (b) 6h, (c) 12h, (d) 24h, (e) 48h.

As far as the growth mechanism is concerned, the effects of TSC must be taken into account. TSC is known to be one of the most powerful general capping agents for the synthesis of nano/microstructures with complex shape and size. Various nanomaterials such as rattle-type hollow carbon spheres, [44] colloidal silver nanoparticles, [45] gold nanoplates, [46] ZnO nanoflowers and coral-like nanocrystals, [47] Cu-InS/ZnS core/shell quantum dots, [48] three-dimensional complex nanostructures, [49] dumbbell and flowerlike hydroxyapatite, [50] are successfully synthesized with the assistance of TSC playing as capping agents, stabilizing agents, modifying agents, directing agents, or soft templates. Under the condition of our experiments, $Al(NO_3)_3$ and $Co(NO_3)_2$ were used as precursors and TSC as stabilizer, and no surfactants were used. The concentration of TSC, which used as capping agent, was found to play an important role in the step-by-step formation of hollow core-shell morphology. As shown in Figure 7a, when TSC was absent in solvent, only wire-like nanobundles can be obtained in final products. When 0.5 mmol of TSC (TSC/Al molar ratio is 0.25) was added to the solution, well-developed core-shell structures with an average diameter of 2-3 μm were observed (Figure 7b). When the TSC/Al molar ratio was increased to 0.5, some irregular pores appear on the surface of the spheres and there are only a few bridges connected between the shell and centre of survived precursor (Figure 7c). When the TSC/Al molar ratio was further increased to 1, little irregular and large solid particles appeared, measuring 3-6 μm, as shown in Figure 7d. As indicated above, although the exact mechanism of the formation of homogeneous core-shell Co_3O_4/Al_2O_3 microspheres is quite difficult to know, it is reasonable to think that a certain amount of TSC in the present reaction system plays a key role in the formation process of core-shell precursor microspheres.

On the basis of the above results, a possible mechanism for the formation of hollow core-shell Co_3O_4/Al_2O_3 microspheres can be explained as follows (also shown schematically in Figure 8). Normally, nanorods should be formed. As shown in Fig. S4 and S5, Al^{3+} and Co^{2+} ions react with deionized water and produce boehmite and cobalt hydroxide phases at higher temperature and pressure without TSC [51]. Finally, 1D AlOOH and $Co(OH)_2$ uniform nanowire bundles with typical lengths of 200-400 nm were formed by the general rolling mechanism [52]. However, in the presence of TSC, the coordination and gradual hydrolysis of TSC with Al(III) and Co(II) would take place, alonging with a slow hydrolysis and growth of aggregated solid microspheres driven by the minimization of the system energy. With time elapsing, Ostwald ripening, defined as "the growth of larger crystals from those of smaller size which have a higher solubility than the larger ones" [53], took place in the aggregated Co-Al hydroxide nanoparticles, and the solid evacuation started underneath the surface layer of the particles. Then the microsphere crystallites would dissolve gradually and diffuse outward to form hexagonal nanorods, which should be structurally more stable for Co-Al hydroxide composites. Voids in the cores of large aggregates gradually form and become bigger, and the shell thickness increases owing to the outward diffusion of solutes through the permeable shell. With the transportation of the mass, the void space between the core and the shell was generated. The hollowing phenomena for crystalline particles through Ostwald ripening have been observed in diverse cases, such as for Fe_3O_4 [54], Cu_2O [55], Bi_2WO_6 [56], $SrZrO_3$[57]. Figure 8 summarizes all major steps during the formation.

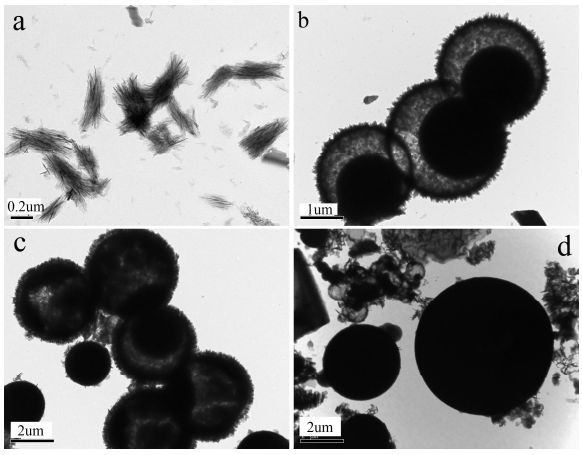

Fig. 7. TEM images of 15wt% Co-loading precursor particles prepared with different TSC/Al molar ratios. (a) 0, (b) 0.25, (c) 0.5, (d) 1.

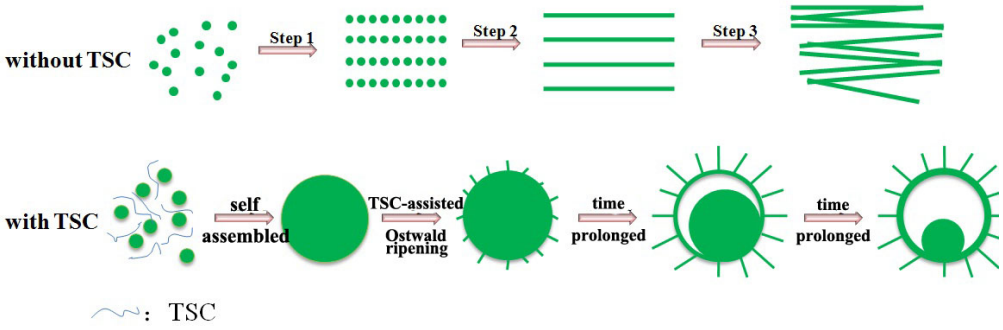

Fig. 8 Schematic illustration of the evolution process of obtained hollow core-shell microspheres.

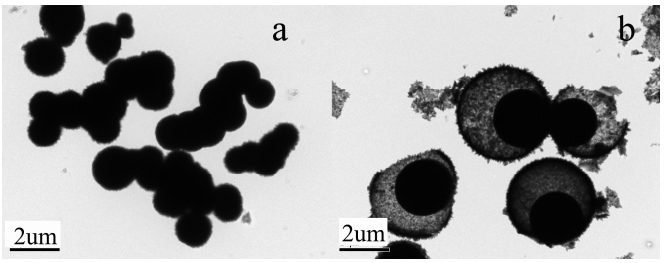

Fig. 9 TEM images of Co_3O_4/Al_2O_3 core-shell microparticles prepared at different temperatures: (a) 160 °C and (b) 220 °C.

Effect of Reaction Temperature. Temperature-dependent experiments were carried out at 160, 200 and 220 °C while keeping all other reaction conditions parallel in 15wt% Co-loading and TSC/Al molar ratio of 0.25 for 24 h. The reaction temperature showed remarkable influence on the morphology of the products. Figure 9a and b show the TEM images of the products obtained at 160 and 220 °C, respectively. When the reaction temperature decreases to 160 °C, only agglomerations assembled from solid spheres with a size in the range of 1-1.5 μm, which extensively agglomerated, can be obtained (Figure 9a). When the reaction temperature increases to 220 °C, cracked core-shell microspheres were formed. Obviously, a higher reaction temperature is beneficial to the synthesis of hollow products. A higher processing temperature can enhance the initial nucleation as well as the aggregation process, [58] and thus favor the formation of initial solid aggregates. Moreover, the following ripening process can also be improved by higher temperature, which can effectively promote the dissolution and diffusion of the species from the particles. Therefore, elevated temperature is a prerequisite for the formation of hollow particles. [59]

Temperature-Programmed Reduction (TPR). The reduction behavior of core-shell Co_3O_4/Al_2O_3 with different Co-loadings was investigated, and the results are shown in Figure 10. As shown in Fig.10, a peak is observed at around 410 °C. According to the previous paper [60], the peak is assigned to the reduction of Co_3O_4 with larger or smaller clusters. The second peak between 600-800 °C can be attributed to the reduction of cobalt oxide in close contact to the alumina support and cobalt aluminates which are only reduced at high temperatures.[61-62] Comparing with S-10, more Co^{2+} in S-15 and S-25 were reduced at high temperature. It was attributed to the presence of well dispersed small cobalt particles which strongly interacted with Al_2O_3 support and even forming the new generated $CoAl_2O_4$ phase and better metal-support bonding with increasing Co-loading. [63]

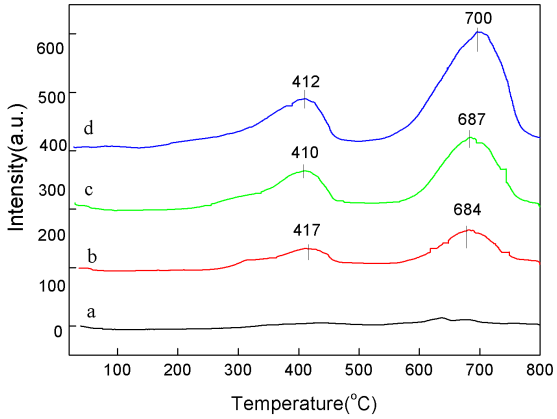

Fig. 10 TPR profiles of Co_3O_4/Al_2O_3 microspheres.
a: S-5; b: S-10; c: S-15; d:S-25.

Table 2. Catalytic activities of the core-shell samples for CO oxidation.

Samples	Pretreatment (°C)	CO oxidation activity $T_{50\%}$ (°C)	CO oxidation activity $T_{90\%}$ (°C)
S-5	500	291	343
S-10	500	239	266
S-15	500	233	257
S-15-400	400	190	209
S-15-600	600	210	228
S-25	500	143	164
10wt%Co (ref.64)	400	380	405
8wt%Co (ref.43)	500	365	450

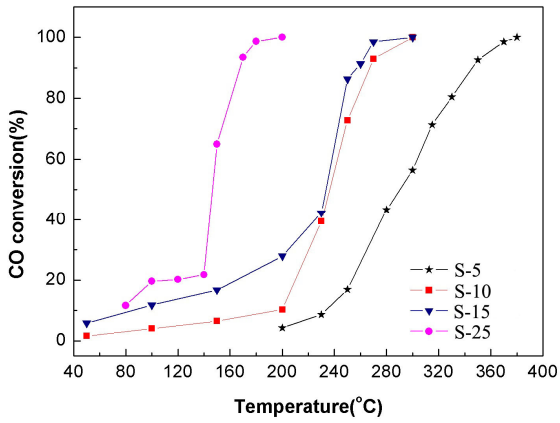

Fig. 11 CO conversion *vs.*reaction temperature curves for the core-shell samples with different Co-loadings. Conditions: flow rate =40 cm^3/min, 3% CO + 12% O_2 balanced by N_2.

As mentioned above, catalytic property is one of the most important properties of Co-Al composite oxides. The catalytic property for CO of core-shell Co_3O_4/Al_2O_3 microspheres with various Co-loadings was studied in a quartz tubular reactor, through which the reaction stream went at a rate of 40ml min^{-1} with 3.0 vol% CO, 12.0 vol% air and 85.0 vol% N_2. Figure 11 and 12 show the catalytic property of the as-fabricated samples, i.e., the CO conversion as a function of reaction temperature. It is observed that CO conversion increased monotonously with the increase in reaction temperature. In order to better evaluate the activities of these samples, the temperatures (T50% and T90%, respectively) required for 50% and 90% CO conversions are employed, as summarized in Table 2. The worst performance for CO combustion, starting at 200 °C and reaching 100% at 382◦C, was achieved over S-5 sample. A slight improvement on oxidation activity was found in the case of S-15 as compared to S-10. From Figure 10 it can be seen that the S-25 ($T_{50\%}$ = 143 °C and $T_{90\%}$ = 164 °C) showed much higher catalytic activity than other samples. Much better CO conversion was observed over core-shell samples sintered at different temperatures. The 15wt% Co-loading sample calcinated at 400°C (labeled as T-400, $T_{50\%}$ = 190 °C and $T_{90\%}$ = 209 °C) was superior in performance to the same amount of Co-loaded Co_3O_4/Al_2O_3 samples sintered at 500°C (labeled as T-500, $T_{50\%}$ = 233 °C and $T_{90\%}$ =257°C) and 600°C (labeled as T-500, $T_{50\%}$ = 210 °C and $T_{90\%}$ = 228 °C). Complete conversion at 300 °C was obtained over T-500. Nevertheless, T-400 and T-600 could lead to an appreciable enhancement giving an entire CO conversion at 225 ◦C and 240 °C. In general, T-400 was verified to be the best active one among the investigated samples. We obtained excellent catalytic capacity of CO in Co_3O_4/Al_2O_3 core-shell microspheres with 2-4 μm in diameter. In the early 2000s, Zeng [64] has examined the CO oxidation performance of Co_3O_4/Al_2O_3 nanopowders with 10 wt% cobalt prepared by sol-gel process, it gives relative lower activity with 50% conversion at 380°C and 100% conversion at as high as 425 °C. Zhang [43] has investigated the Co_3O_4/Al_2O_3 nanopowders with 8% Co-loading prepared by precipitation method, CO conversion was 50% at 380°C and reached 90% at 450 °C. In general, core-shell Co_3O_4/Al_2O_3 microspheres were verified to be the best active catalyst among the investigated samples. This may be attributed to the extremely large surface area and pore volume and the narrow pore-size distribution, which greatly enhance its potential applications as an ordered mesoporous Co_3O_4/Al_2O_3 catalyst. But the exact correlation between the structure and activity behavior of catalytic performance requires further theoretical and experimental work.

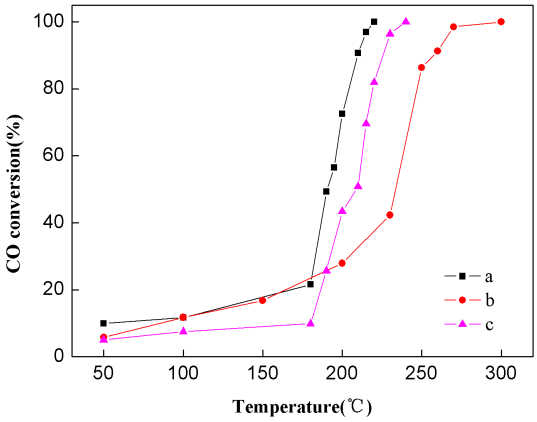

Fig. 12 CO conversion *vs.*reaction temperature curves for the core-shell Co_3O_4/Al_2O_3 samples calcinated at (a) 400 °C; (b) 500 °C; (c) 600°C. Condition: 15wt% Co-loading, flow rate =40 cm^3/min, 3% CO + 12% O_2 balanced by N_2.

4. Conclusion

In summary, a facile template-free hydrothermal method for synthesis of Co_3O_4/Al_2O_3 microspheres with size about 2-4 μm has been reported. On the basis of the experimental results, a TSC-assisted Ostwald ripening process has been proposed as the possible mechanism for the formation of core-shell structures. A certain concentration of TSC plays a key role in the formation of hollow core-shell microspheres. The hollow nature and the shell composed of intercrossed nanorods provide a high BET surface area and active catalytic abilities, which leading to an excellent catalytic activity for CO oxidation. This method provides a simple route for synthesizing metal-doped alumina hollow structures and could be extended to other material systems.

Acknowledgements

This work is financial supported by China Postdoctoral Science Foundation, Alliance Plan (problem public bidding project: LM201334), the National Natural Science Foundation of China (NO. 21273145) and National Science Foundation for Distinguished Youth Scholar (grant NO. 51325203).

Notes and references

*Address: 311 Room, HA building, 99 Shangda Road, Shanghai, 200444, China. Tel.: +86 21 6613 8066. Fax: +86 21 6613 3513. E-mail: lmzhang@mail.shu.edu.cn (L.M.Zhang), wclu@shu.edu.cn (W.C.Lu)

[a]Shanghai Institute of Ceramics (SIC), Chinese Academy of Sciences (CAS), Dingxi 1295, Shanghai 200050, China

[b]Department of Chemistry, School of Science, Shanghai University, Shanghai 200444, China

[c] School of Materials Science and Engineering, Shanghai University, Shanghai 200444, China

†Electronic Supplementary Information (ESI) available: XRD patterns of the samples T-400, T-500, T-600, IR and Raman spectra are shown in Figure S1, S2 and S3, respectively. XRD patterns and TEM images of the samples without TSC collected at different time are shown in Figure S4 and S5.

(1) G. C. Rajib, P. Santanu, *Chem. Rev.*, 2012, **112**, 2373.
(2) J. Hu, M. Chen, X. S. Fang, L. M. Wu, *Chem. Soc. Rev.,* 2011, **40**, 5472.
(3) Y. D. Liu, J. Goebl, Y. D. Yin, *Chem. Soc. Rev.*, 2013, **42**, 2610.
(4) X. W. Lou, L. A. Archer, Z. Yang, *Adv. Mater.* 2008**, 20**, 3987.
(5) Z. H. Xu, Y. Gao, T. Liu, L. M. Wang, S. S. Bian, J. Lin, *J. Mater. Chem.*, 2012, **22**, 21695.
(6) M. F. Shao, F. Y. Ning, J. W. Zhao, M. Wei, D. G. Evans, X. Duan, *J. Am. Chem. Soc.* 2012**, 134**, 1071.
(7) J. B. Zhou, C. Tang, B. Cheng, J. G. Yu, M. Jaroniec, *ACS Appl. Mater. Interfaces* 2012, **4,** 2174.
(8) Y. Xia, Z. Xiao, X. Dou, H. Huang, *ACS Nano,* 2013, **7**, 7083.
(9) W. D. Shi, S. Y. Song, H. J. Zhang, *Chem. Soc. Rev.*, 2013, **42**, 5714.
(10) R. Ameloot, F. Vermoortele, W. Vanhove, M. B. J. Roeffaers, B. F. Sels, V. D. E. De, *Nat. Chem*. 2011**, 3**, 382.
(11) C. X. Cao, Y. F. Gao, L. T. kang, H. J. Luo, *CrystEngComm.*, 2010, **12**, 4048.
(12) G. L. Li, H. Möhwald, D. G. Shchukin, *Chem. Soc. Rev.*, 2013,**42**, 3628.
(13) Y. J. Xiong, B. Wiley, J. Y. Chen, Z. Y. Li, Y. D. Yin, Y. N. Xia, *Angew. Chem., Int. Ed.* 2005, **44,** 7913.
(14) D. Kim, J. Park, K. An, N. K. Yang, J. G. Park, T. Hyeon, *J. Am. Chem. Soc.*2007, **129**, 5812.
(15) K. Y. Niu, J. Park, H. Z. M. Zheng, A. P. Alivisatos, *Nano Lett.* 2013, **13***,* 5715.
(16) W. S. Wang, M. Dahl, Y. D. Yin, *Chem. Mater.* 2013**, 25**, 1179.
(17) C. C. Yec, H. C. Zeng, *J. Mater. Chem. A* 2014, DOI: 10.1039/c3ta14203e.
(18) P. Tartaj, J. M. Amarilla, *Chem. Commun.*, 2014, **50**, 2077.
(19) J. Hu, M. Chen, X. S. Fang, L. M. Wu, *Chem. Soc. Rev.*, 2011,**40**, 5472.
(20) X. Y.Chen, M. H.Qiao, S. H.Xie, K. N. Fan, *J. Am. Chem. Soc.* 2007, **129,** 13305.
(21) Li, H. X.; Bian, Z. F.; Zhu, J.; Zhang, D. Q. *J. Am. Chem. Soc.* **2007,** *129*, 8406-8407.
(22) Xu, Y. Y.; Jiao, X. L.; Chen, D. R. *J. Phys. Chem. C,* **2008,** *112 (43),* 16769-16773.
(23) L. M.Zhang, W. C. Lu, *Materials Research Bulletin,* 2010, **45**,429.
(24) L. M.Zhang, W. C.Lu, L. M.Yan, Y. L.Feng, *Microporous and Mesoporous Materials,* 2009, **119***,* 208.
(25) M.Llusar, A.Fores, J. A.Badenes, J.Calbo, M. A.Tena, G. Monros, *J. Eur. Ceram. Soc.* 2007**, 21,** 1121.
(26) Z.Wang, C.Chen, T.Zhang, H.Guo, B.Zou, R.Wang, F. Wu, *Sens. Actuators B* 2007, **124**, 678.
(27) L. F. Liotta, H. J. Wu, G.Pantaleoa, A. M. Venezia, *Catal. Sci. Technol.,* 2013, **3**, 3085.
(28) L. H.Su, X. G. Zhang, Y. Liu, *J. Solid State Electrochem.,* 2008, **12**, 1129.
(29) M. Sales, C.Valentin, J. Alarcon, *J. Eur. Ceram. Soc.,* 1997, **17**, 41.
(30) C. O. Arean, M. P. Mentruit, E. E. Platero, F. L. Xamena, J. B. Parra, *Mater. Lett.* 1999, **39**, 22.
(31) M. T. Lodge, P. P. Edwards, P. A. Anderson, M. O. Jones, I. Gameson, *Polyhedron* 2006**, 25**, 568.
(32) W. S. Cho, M. Kahihana, *J. Alloys Compd.* 1999, **287**, 87.
(33) N. Ouahdi, S. Guillemet, J. J. Demai, B. Durand, *Mater. Lett.* 2005, **59***,* 334.
(34) Z.Z.Chen, E.W.Shi, W. J. Li, Y. Q. Zheng, J. Y. Zhuang, B. Xiao, L. A. Tang, *Mater. Sci. Eng. B* 2004, **107***,* 217.
(35) C.Wang, S. Liu, L. Liu, X. Bai, *Mater. Chem. Phys.* 2006**, 96**, 361.

(36) S. Mmartyotin, U. S. Sangngern, A. Kaewvilai, N. Koonsaeng, H. Manuspiya, A. Laobuthee, *J. Sustainable Energy & Environment* 2009, **1,** 31.
(37) L. Ji, J. Lin, H. C. Zeng, *J. Phys. Chem. B* 2000, **104**, 1783.
(38) C. H. He, M. Paulus, W. Chu, J. Find, *Catalysis Today* 2008, **131**, 305.
(39) W. J. Wang, Y. W. Chen, *Appl. Catal.* 1991, **77**, 223.
(40) G. Busca, V. Lorenzelli, V. Bolis, *Mater., Chem. Phys.* 1992, **31,**221.
(41) S. Chokkaram, R. Srinivasan, D. R. Milburn, B. H. Davis, *J.Mol. Catal. A* 1997, **121,** 157.
(42) W. Di, X. Ren, H. Zhao, N. Shirahata, Y. Sakka, W. Qin, *Biomaterials* 2011, **32**, 7226.
(43) R. D. Zhang, P. X. Li, N. Liu, W. Yang, X. D. Wang, R. Cui, B. H. Chen, Catalysis Today 2013, **216** , 169.
(44) R. B. Zheng, X. W. Meng, F. Q. Tang, L. Zhang, J. Ren, *J. Phys. Chem. C* 2009, **113**, 13065.
(45) S. Agnihotri, S. Mukherji, S. Mukherji, RSC Adv., 2014, 4, 3974.
(46) S. A. Chil, J. Y. Yong, J. P. Hyung, W. J. Kim, H. H. Dong, S. Y. Wan, *Chem. Mater.*, 2005, **17**, 5558.
(47) G. Q. Yuan, J. B. Zhu, C. H. Li, X. F. Gao, *CrystEngComm*, 2012, **14**, 7450.
(48) Y.Y. Chen, S. J. Li, L. J. Huang, D. C. Pan, *Inorg. Chem.*, 2013, **52**, 7819.
(49) L. C. Yang, Y. S. Lai, C. M. Tsai, Y. T. Kong, C. Lee, C. L. Huang, *J. Phys. Chem. C*, 2012, **116**, 24292.
(50) H. Yang, L. J. Hao, C. Du, Y. J. Wang, *RSC Adv*., 2013, **3**, 23184.
(51) Y.L. Feng, W.C. Lu, L.M. Zhang, X. H. Bao, B.H. Yue, Y. lv, X.F. Shang, *Cryst. Growth Des.*, 2008, **8**, 1426.
(52) X. Y. Chen, H. S. Huh, S.W. Lee, *Nanotechnology* 2007, **18**, 285608.
(53) W. Z. Ostwald, *Phys. Chem.* 1897, **22**, 289.
(54) W. Cheng, K. B. Tang, Y. X. Qi, J. Sheng, Z. P. Liu, *J. Mater. Chem.,* 2010, **20**, 1799.
(55) B. Y. Geng, J. Liu, Y. Y. Zhao, C. H. Wang, *CrystEngComm*, 2011,**13**, 697.
(56) C.C. Mao, M. L. Li, Z. G. Fang, F. L. Meng, X. N. Qu, Y. P. Liu, M . J. Wang, J. Zhang, Z. Shi, X. H. Guo, *RSC Advances*, 2013, **3**, 6631.
(57) T. N. Ye, Z. H. Dong, Y. N. Zhao, J. G. Yu, F. Q. Wang, S. K. Guo, Y. C. Zou, *CrystEngComm*, 2011, **13**, 3842.
(58) J. W. Mjuulin, Crystallization; Butterworth: London, 1961.
(59) X. L. Tian, J. Li, K. Chen, J. Han, S. L. Pan, Y. J. Wang, X. Y. Fan, F. Li, Z. X. Zhou, *Crystal Growth & Design,* 2010, **10**, 3990.
(60) S. M. Kim, J. W. Bae, Y. J. Lee, K. W. Jun, *Catal. Comm.* 2008, **9**, 2269.
(61) B. Jongsomjit, G. Li, B. H. Racoillet, Davis, *Appl. Catal., A,* 2002, **233**, 263.
(62) M. Minnermann, B. Neumann, V. Zielasek, M. Bäumer, *Catal. Sci. Technol.,* 2013, **3**, 3256.
(63) R. D. Zhang, P. X. Li, N. Liu, W. Yang, X. D. Wang, R. Cui, B. H. Chen, *Catalysis Today* 2013, **216**, 169.
(64) L. Ji, J. Lin, H. C. Zeng, *J. Phys. Chem.* B 2000, **104**, 1783.

Solvothermal Synthesis of Co_3O_4/Al_2O_3 Hollow Core-shell Microspheres for Catalytic Oxidation of CO

Liangmiao Zhang[1*], Taiang Liu[2], Xin Zhao[2], Na Qian,[2] Pan Xiong[2], Wenjing Ma,[2] Wencong Lu[2*], Yanfeng gao[3], Hongjie Luo[1,3]

[1] Shanghai Institute of Ceramics (SIC), Chinese Academy of Sciences (CAS), Dingxi 1295, Shanghai 200050, China

[2] Department of Chemistry, School of Science, Shanghai University, Shanghai 200444, China

[3] School of Materials Science and Engineering, Shanghai University, Shanghai 200444, China

Shape-controlled synthesis of Co_3O_4/Al_2O_3 hollow core-shell microspheres has been achieved by solvothermal process in a mixed solvent of water and acetone, which exhibited excellent CO catalytic performance due to their large surface area and mesoporous structures.

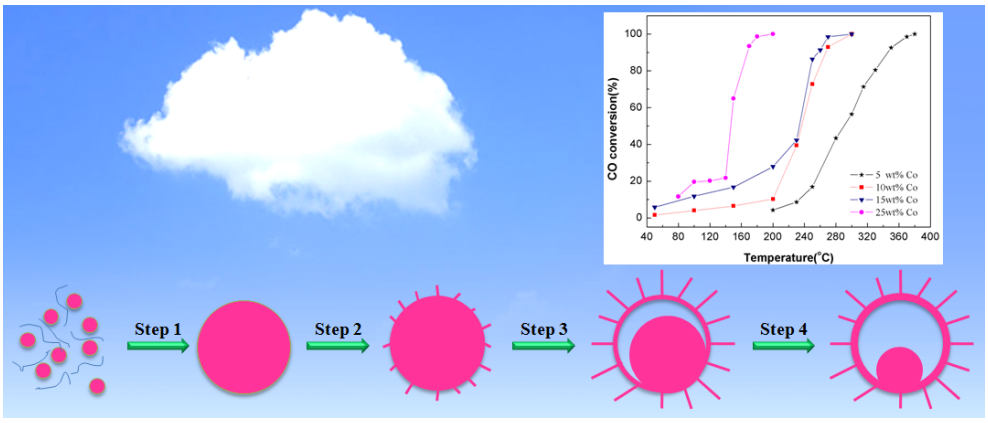

* Corresponding author. Tel: +86-21-66138066; fax: +86-21-66133513.

E-mail: zlmldy@163.com (L.M.Zhang); wclu@shu.edu.cn (W.C.Lu)